Modeling and experimental investigation on the fuel particle heat-up and devolatilization behavior in a fluidized bed

Ke, Xiwei; Engblom, Markus; Cheng, Lu; Chen, Lujian; Cai, Runxia; Hupa, Leena; Lyu, Junfu; Yang, Hairui; Zhang, Man

Published in:
Fuel

DOI:
10.1016/j.fuel.2020.119794

Published: 15/03/2021

Modeling and experimental investigation on the fuel particle heat-up and devolatilization behavior in a fluidized bed

Xiwei Ke[a], Markus Engblom[b], Lu Cheng[a], Lujian Chen[a], Runxia Cai[a], Leena Hupa[b], Junfu Lyu[a], Hairui Yang[a], Man Zhang[a, *]

[a]*Key Laboratory for Thermal Science and Power Engineering of Ministry of Education, Department of Energy and Power Engineering, Tsinghua University, Beijing 100089, China*

[b]*Process Chemistry Centre, Åbo Akademi University, Biskopsgatan 8, 20500 Turku, Finland*

* *Corresponding author Tel: +86-10-62773384 E-mail address: zhangman@mail.tsinghua.edu.cn*

Abstract

The proper understanding and description of fuel devolatilization behavior in a fluidized bed (FB) is important to the FB reactor design and modeling. Aiming at this issue, two different mathematical models, isothermal (0D) particle model and one-dimensional (1D) particle model, have been developed. The particle heat transfer is solved simultaneously using an iterative approach with the existing nitrogen containing chemical percolation devolatilization (CPD-NLG) model. Experiments in a special designed FB reactor were conducted to help validate both the temperature solver and modifications to the fast nitrogen release chemical kinetic parameters. The results show that when the bed temperature is higher or coal size become smaller, the final volatiles yield increases and the nitrogen remaining in char decreases. Under all conditions given in the present study, the final nitrogen content of char is always lower than that of parent coal. The yields of some volatile species are also affected by the coal size and bed temperature. In addition, simulation analysis reveals that the deviation between the results of these two models cannot be ignored if the particle size exceeds a specific value (transition

size), namely, the large particle is improper to be described as isothermal during heat-up, while this transition size decreases with the increase of bed temperature. A selection principle of these two models is proposed for balancing the calculation precision and computational time. The particle model developed in this work makes it possible to carry out further FB reactor simulations with the devolatilization process more consistent with laboratory data.

Keywords: Devolatilization, Fluidized bed, Modeling, Particle size, Temperature

Introduction

The fuel particles undergo drying and devolatilization as the first step after they are introduced into the fluidized bed (FB) at which the particles decompose into char, tar and several light gas species. Though the devolatilization usually completes in a very short time compared to the subsequent char reaction process, it has significant effects on the characteristics of several fuel thermal conversion processes, including combustion, gasification and nitrogen oxide formation [1-3]. Therefore, the proper understanding and description of fuel devolatilization behavior is a very key issue in both chemical reactor design and modeling.

Several models have been proposed to simulate the devolatilization process of fuel particles, including constant rate model [4], single kinetic rate model [5], two competing rates (Kobayashi) model [6], distributed activation energy (DAE) model [7]. Bu [8] and Sadhukhan [3] both use the DAE model for simulating the pyrolysis of a single fuel particle in the FB. Chen [9] assumed the lignite washery tailing particles' devolatilization process consists of 6 kinetic reactions which can all be formulated by first order kinetic expressions. However, these

models can only provide the information of devolatilization rate, some other important characteristics such as the volatile species distribution were ignored. To analyze the fuel devolatilization behavior comprehensively, one of the network models, chemical percolation devolatilization (CPD) containing nitrogen and light gas release (NLG) model that was developed by Fletcher et al. [10-13], is applied in this paper. It has been validated in many studies [14, 15] and widely used in coal and biomass simulations [16-18]. The CPD-NLG model assumes the compositions of initial volatiles are tar, H_2O, CO_2, CH_4, CO, nitrogen-containing light gas and some $C2^+$ light hydrocarbons, which are also the most frequently reported major volatile species [19-23].

Other than the conversion of elements C, H, O, the fuel nitrogen is accordingly partitioned into char-N and volatile-N during devolatilization. Numerous studies have been conducted with the quest to determine the char-N / volatile-N distribution due to its significant effect on the NO_x emission of a FB reactor [24-26]. Some studies report that the nitrogen content in char will be higher than that of the parent coal, especially for the low degree of devolatilization, i.e. low final temperature and short residence time [27, 28]. However, some other experimental research present contradicting results [2]. A proper description of the fuel-N release under different conditions is also a key point in FB modeling and prediction of NO_x emission.

The CPD-NLG model needs the particle temperature as the input data, hence the heat transfer process of a spherical particle in the FB should be simulated simultaneously. Salmasi et al. [16] used Computational Fluid Dynamics (CFD) to simulate the temperature history of a single coal particle during devolatilization, and they pointed out that the energy exchange

between inert bed materials and fuel particle cannot be ignored in the FB. However, CFD modeling is very time-consuming. Instead, there are two typical mathematical models to describe the particle thermal conversion process: isothermal particle model (lumped parameter method, 0D) [16, 18] and one-dimensional particle model (1D) [3, 9]. The former assumes the particle is thermally thin, namely, the temperature is uniform throughout the particle at any given time. While the latter considers a thermally thick particle, inside which the temperature, as well as the devolatilization or combustion process, is uneven, thus the spatial terms need to be discretized in solving (assuming that the coal particle is isotropic). Though the 0D model is simpler and costs shorter computational time, the 1D particle model is more realistic as revealed in the study of Ström and Thunman [29]. Therefore, there should be a balance between the calculation precision and computational efficiency when selecting the particle model.

The fuel devolatilization characteristics are affected by many factors, including particle size [3, 16, 23, 30-33] and shape [34], environmental temperature [2, 3, 9, 16, 17, 19, 21, 22, 30, 34-36], heating rate [17, 20, 23, 32], fuel type(rank) [2, 21, 31, 34], atmosphere [1, 31, 32, 36], etc. Tian et al. [23] and Yan et al. [17] both argued that the temperature and fuel particle size are the more important parameters compared to others. For example, larger fuel particles experience lower heating rate and uneven heating [16, 30], resulting in longer devolatilization time [30, 34] and different yields of volatiles [3, 23, 33]. Further, with the higher environment/surrounding temperature, the devolatilization time is shorter [3, 30, 34] and the volatiles yield is higher [3, 21, 22, 35, 37]. In addition, the composition of volatiles, as well as the distribution of fuel-N into volatile-N and char-N, may also change [2, 17, 19, 21, 31].

The present study aims at establishing a mathematical model for fuel devolatilization behavior in a fluidized bed with high efficiency in terms of computational time. This model can predict the yields of volatiles including the release of volatile-N, while the particle heat-up process has significant effects on the fuel devolatilization characteristics. Two different simple models, isothermal (0D) particle model and one-dimensional (1D) particle model, have been developed and compared. The particle heat transfer is solved simultaneously using an iterative approach with the existing CPD-NLG model. Experiments in a special designed FB reactor were conducted to help validate both the temperature solver and modifications to the fast nitrogen release chemical kinetic parameters. Besides, the effects of the coal particle size and bed temperature on the fuel particle heat-up and devolatilization behavior are also discussed.

2. Mathematical model

2.1 CPD model and devolatilization rate

The CPD-NLG model is applied in this paper as the kinetic model to describe the single fuel particle devolatilization behavior based on the chemical structure of parent fuel. Five parameters about the chemical structure that are directly measured by 13-C NMR spectroscopy, M_{cl}, M_{del}, σ+1, p_0 and c_0, should be determined before utilizing the CPD-NLG model. Fletcher et al. have developed a correlation to derive these parameters from a combination of the elemental and proximate analyses. A more detailed description of the CPD-NLG model and the parameter correlation is found elsewhere [10-12, 14, 15, 38].

104 The output variables from the CPD-NLG program include the time series of total volatiles
105 yield ($Y_{\mathrm{Vol,daf}(j,k)}$) and each volatile species yield ($Y_{\mathrm{Vol,daf}(j,k,m)}$) (in dry ash-free basis). Hence, the
106 final volatiles yield for j_{th} size fuel particles in received basis can be expressed as:

107 $$Y_{\mathrm{final,Vol,ar}(j)} = \gamma_{\mathrm{daf}} Y_{\mathrm{Vol,daf}(j,k=N_k)} \tag{1}$$

108 where Y represents the yield mass fraction, subscripts j, k, m, Vol denote the fuel particle size
109 group, fuel particle age group, volatile species number and volatiles, respectively. γ_{daf} is the
110 content of char plus volatiles in fuel, $\gamma_{\mathrm{daf}} = 1 - Y_{\mathrm{ash,\,Fuel,\,ar}} - Y_{\mathrm{H_2O,\,Fuel,\,ar}}$.

111 The devolatilization is considered complete when the yield of total volatiles reaches 95%
112 of the final volatiles fraction. Assuming that the final char consists of carbon and ash only, the
113 final N/C ratio in the char, normalized to the N/C ratio in the parent coal, can be written as
114 follows:

115 $$\theta_{\mathrm{N/C}(j)} = \frac{Y_{\mathrm{N,Fuel,ar}}\varphi_{\mathrm{N,char}(j)}}{\gamma_{\mathrm{daf}}\left(1 - Y_{\mathrm{Vol,daf}(j)}\right)} \cdot \frac{Y_{\mathrm{C,Fuel,ar}}}{Y_{\mathrm{N,Fuel,ar}}} = \frac{\varphi_{\mathrm{N,char}(j)} Y_{\mathrm{C,Fuel,ar}}}{\gamma_{\mathrm{daf}}\left(1 - Y_{\mathrm{Vol,daf}(j)}\right)} \tag{2}$$

116 where $\varphi_{\mathrm{N,char}}$ represents the mass fraction of nitrogen remaining in the char, which is also one
117 of the output variables from the CPD-NLG program. If $\theta_{\mathrm{N/C}}$ is greater than 1, it means that the
118 char is enriched in nitrogen. Conversely, more fuel-N is supposed to be released as volatiles.

119 *2.2 Single particle heat transfer model*

120 This section introduces the mathematical approaches of the two single fuel particle heat
121 transfer models: isothermal particle model (0D) and one-dimensional particle model (1D). Note
122 that in order to eliminate the influence of the discrepancy of moisture content among different

size raw fuel particles, in this paper, the studied fuel particles are dried before experiments, thus the item about water vaporization is ignored in the particle energy balance equations.

2.2.1 Isothermal particle heat transfer model (0D model)

The overall heat transfer Q between the particle surface and the outside environment is expressed as the sum of three parts: solid particle convective heat transfer Q_{sc} (from surrounding bed materials to fuel particles), gas convective heat transfer Q_{gc} and radiative heat transfer Q_r. Therefore, the energy conservation equation of an isothermal particle in the FB is written as follows:

$$m_p c_p \frac{dT_p}{dt} = h_{gc} A_p \left(T_g - T_p\right) + h_{sc} A_p \left(T_s - T_p\right) + A_p \kappa_p \sigma \left(T_e^4 - T_p^4\right) + \frac{dm_{Vol}}{dt} \Delta H_{devol} \quad (3)$$

where m denotes the mass, c denotes the specific heat capacity, T represents the temperature, A_p is the particle surface area, κ is effective the surface emissivity, σ is the Stefan-Boltzmann constant, h_{gc} and h_{sc} denotes the heat transfer coefficients of gas convection and solid particle convection, respectively ($h_c = h_{gc} + h_{sc}$), ΔH_{devol} is the pyrolysis reaction heat, subscripts *s*, *p*, *g*, *e* represent the inert bed materials, fuel particle, gas phase and environmental parameters, respectively.

In this paper, we consider that the radiative heat transfer is between a grey body (the fuel particle) and a black body (the bed), and the radiative heat flux is dominated by emission from the relatively low temperature particle layer in the vicinity of the heat receiving surface. Because of the "cavity effect", the effective surface emissivity of the fuel particles (κ_p) is a little higher than that of the particles themselves [39, 40], and the κ_p is assumed as a constant value

143 (=0.85), hence the four-fold Stephan-Boltzmann law written in Equ.(3) which describes the
144 radiation is still valid in the present context. Besides, the temperature in a bubbling fluidized
145 bed (T_{bed}) is very uniform and stable, namely, $T_g = T_s = T_e = T_{bed}$.

146 The gas convective heat transfer coefficient h_{gc} is correlated to the Nusselt number (Nu),
147 which is expressed by Prandtl number (Pr) and Reynolds number (Re):

148
$$\begin{cases} \mathrm{Nu} = h_{gc} d_p / \lambda_g = 2.0 + 0.6\,\mathrm{Re}^{0.5}\,\mathrm{Pr}^{1/3} \\ \mathrm{Re} = \rho_g U_{mf,s} d_p / \left(\mu_g \varepsilon_{mf,s}\right) \\ \mathrm{Pr} = c_g \mu_g / \lambda_g \end{cases} \tag{4}$$

149 where μ is the dynamic viscosity, λ is the heat conduction coefficient, U_{mf} is the minimum
150 fluidization velocity, $\varepsilon_{mf,s}$ is the minimum bed voidage which is calculated by the following
151 correlation [41]:

152
$$\varepsilon_{mf} = \frac{0.586}{\phi_s^{0.72}} \left(\frac{\rho_g}{\rho_s}\right)^{0.021} \left[\frac{\mu_g^2}{\left(\rho_s - \rho_g\right)\rho_g d_p^3 g}\right]^{0.029} \tag{5}$$

153 The solid particle convective heat transfer plays an important role in the overall heat
154 transfer process [16] in the FB, which can be expressed as a combination of the contact thermal
155 resistance R_{cont} and the thermal resistance of a thermal penetration layer R_{pene} [42]:

156
$$h_{sc} = \frac{1}{R_{cont} + R_{pene}} \tag{6}$$

157 The penetration layer thermal resistance, R_{pene}, is expressed as

158
$$\begin{cases} R_{pene} = 0.5\sqrt{\dfrac{\pi\theta_t}{\lambda_s \rho_{em} c_{s,em}}} \\ \theta_t = 0.318\left[\left(2\times10^5 d_s + 24.6\right)d_p - 93.3 d_s + 0.154\right]\left(U_g - U_{mf}\right)^{-0.610} \end{cases} \tag{7}$$

159 where λ_s is the effective thermal conductivity of emulsion; ρ_{em} is the emulsion density; $c_{s,em}$ is
160 the specific heat capacity of emulsion phase; θ_t denotes the mean emulsion residence time.

The R_{pene} is more suitable for the continuous contact and long residence time. For the heat transfer process in the case of large coal particles or short residence time, another effect, surface contact resistance R_{cont}, becomes more obvious:

$$\begin{cases} R_{cont} = d_s / \left(N_s \lambda_g \right) \\ N_s = 2.5\ln\left(d_p / d_s \right) + 2, \;\; d_p > d_s \exp^{-0.8} \end{cases} \quad \begin{cases} R_{cont} \to \infty \;\; \& \;\; h_{sc} = 0 \\ N_s \to 0, \;\; d_p \le d_s \exp^{-0.8} \end{cases} \tag{8}$$

where d_s is the inert bed materials size; λ_g is the thermal conductivity of gas; N_s denotes the surface thermal contact resistance constant.

It should be noted that the particle convective contribution toward the total heat transfer will be limited if the fuel particle size is close or even smaller than the surrounding particles, due to the tendency of synchronous particle movement in a bubbling fluidized bed [39]. Both considering the reasonability and the continuity of equation, for the extremely fine fuel particles ($d_p < d_s e^{-0.8}$), the contact thermal resistance (R_{cont}) approaches infinity and the particle convective heat transfer coefficient (h_{sc}) is nearly zero, as expressed in Equ.(8).

The calculated convective heat transfer coefficients, h_{gc}, h_{sc} and $h_{gc}+h_{sc}$, as a function of coal particle size are shown in Fig. 1. It shows that the h_{sc} will decrease sharply if d_p is close to the surrounding bed materials, and the particle heat transfer will not be affected by the particle convection when d_p is smaller than a specific value.

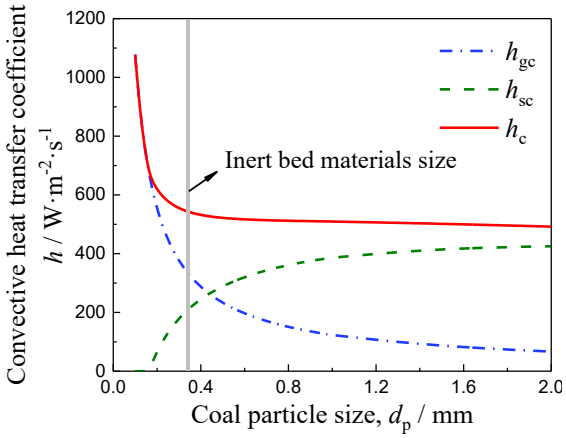

177

178 **Fig. 1 Calculated convective heat transfer coefficients as a function of coal particle size**

179 **(Bubbling fluidized bed conditions as listed in Tab. 3, T_{bed} = 850°C)**

180 Assuming that the particle size d_p remains unchanged during devolatilization, while the

181 particle mass m_p gradually decreases due to the loss of volatiles:

182
$$\begin{cases} m_{p(k)} = m_{p,0} - \gamma_{daf}\left(1 - Y_{Vol,daf(k)}\right)m_{p,0} \\ m_{p,0} = \rho_{p,0} \cdot \dfrac{1}{6}\pi d_p^3 \end{cases} \tag{9}$$

183 where $m_{p,o}$ is the initial fuel particle mass, ρ_p is the fuel particle density. Hence, there is also a

184 mass time series for a fuel particle, and it should be determined by iteration between heat

185 transfer model and CPD model.

186 Equ.(3) is solved analytically by assuming that the particle temperature and mass do not

187 change significantly during a time step:

188
$$\begin{cases} T_p\left(t+\Delta t\right) = \alpha_p + \left[T_p\left(t\right) - \alpha_p\right]\exp\left(-\beta_p \Delta t\right) \\ \alpha_p = \dfrac{hA_pT_g + A_p\kappa_p\sigma T_e^4 + \dfrac{\Delta m_{Vol}}{\Delta t}\Delta H_{devol}}{hA_p + A_p\kappa_p\sigma T_p^3}, \quad \beta_p = \dfrac{A_p\left(h + \varepsilon_p\sigma T_p^3\right)}{m_p c_p} \end{cases} \tag{10}$$

In the calculation of 0D particle heat transfer model, the time step Δt is set to be 0.5 ms. Using this value typically resulted in time step temperature changes (dT/T) smaller than 5% even for very fine particle (100 μm) at high temperature (900℃).

2.2.2 one-dimensional particle heat transfer model (1D model)

The heat transfer equation of an isotropous particle is written as:

$$\rho_{\mathrm{p}} c_{\mathrm{p}} \frac{\partial T_{\mathrm{p}}}{\partial t} = \frac{1}{r^2} \frac{\partial}{\partial r} \left(\lambda_{\mathrm{p}} r^2 \frac{\partial T_{\mathrm{p}}}{\partial r} \right) + \dot{\zeta}_{\mathrm{devol}} \tag{11}$$

The boundary conditions of the energy conservation equation are as follows:

$$\begin{cases} \lambda_{\mathrm{p}} \left. \dfrac{\partial T_{\mathrm{p}}}{\partial r} \right|_{r=0} = 0 \\ \lambda_{\mathrm{p}} \left. \dfrac{\partial T_{\mathrm{p}}}{\partial r} \right|_{r=r_{\mathrm{p}}} = h_{\mathrm{gc}} A_{\mathrm{p}} \left(T_{\mathrm{g}} - T_{\mathrm{p}} \right) + h_{\mathrm{sc}} A_{\mathrm{p}} \left(T_{\mathrm{s}} - T_{\mathrm{p}} \right) + A_{\mathrm{p}} \kappa_{\mathrm{p}} \sigma \left(T_{\mathrm{e}}^4 - T_{\mathrm{p}}^4 \right) \end{cases} \tag{12}$$

where the h_{gc} and h_{sc} are calculated in the same way as 0D model.

The concentric annular layer scheme is used for the space discretization, as displayed in Fig. 2. The specific mesh size depends on the particle size. A finer mesh is used for smaller particles, while, considering the computational efficiency, the minimum mesh size is preferably larger than 12.5 μm, meanwhile, the maximum mesh number should be lower than 50. The first order explicit method is applied in solving Equ.(11), and the length of time steps is controlled by the CFL condition to avoid divergence (CFL = 0.1).

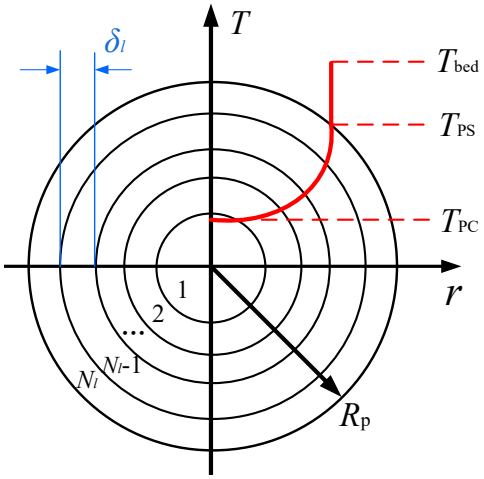

Fig. 2 Schematic of the one-dimensional fuel particle devolatilization model

After meshing, a fuel particle can be regarded as consisting of several layers and each layer is assumed to be uniform. Due to the temperature gradients inside a particle, the devolatilization occurs sequentially in a given layer as the local temperature increases. When the calculation of heat transfer model completes, each layer can obtain its own time series of temperature. Meanwhile, each layer had respective initial mass (the initial temperature is the same). Therefore, the devolatilization processes of different layers can be calculated by CPD model separately. Each layer also has a mass time series which is used as the iterative value.

The net yield of volatiles from a whole fuel particle is expressed as:

$$Y_{\mathrm{Vol,daf}(k,m)} = \sum_{l=1}^{N_{l,\mathrm{p}}} \chi_{\mathrm{V}(l)} Y_{\mathrm{Vol,daf}(k,m,l)} \tag{13}$$

where $\chi_{\mathrm{V}(l)}$ is the volume fraction of l_{th} layer, $N_{\mathrm{l,p}}$ is the number of layers.

The value of some common parameters used in both 0D and 1D particle models are listed in Tab. 1. For the model developed in this paper, the main input parameters are fuel particle properties (elemental and proximate analyses, sphericity, size, particle density), inert bed

219 material (quartz sand) properties (size, sphericity, particle density) and operation conditions
220 (temperature, fluidization velocity).

221 **Tab. 1 Parameters and their value in particle heat transfer models (both 0D and 1D)**

Parameter	Unit	Value	Source
$\rho_{p,0}$*	kg·m^{-3}	1500	assumed
κ_p	-	0.85	assumed
σ	W·m^{-2}·K^{-4}	5.67×10^{-8}	constant
c_p	J·kg^{-1}·K^{-1}	$420 + 2.1T_p + 6.85\times10^{-4}\times T_p^2$	[9]
λ_p	W·m^{-1}·K^{-1}	$5\times10^{-4}\,(T_p - 273.15) + 0.1104$	[43]
c_s	J·kg^{-1}·K^{-1}	$T_g \le 847$K: $(-6.076591 + 0.2516755T_g - 3.247964\times10^{-4}T_g^2 + 1.685604\times10^{-7}T_g^3 + 2548/T_g^2)/60.08\times10^3$; $T_g > 847$K: $(58.75340 + 1.027925\times10^{-2}T_g - 1.31384\times10^{-7}T_g^2 + 2.5210\times10^{-11}T_g^3 + 25601/T_g^2)/60.08\times10^3$	NIST Chemistry WebBook (quartz)
λ_s	W·m^{-1}·K^{-1}	3.8	[44]
$c_{g,Ar}$	J·kg^{-1}·K^{-1}	$(20.786 + 2.825911\times10^{-10}T_g - 1.464191\times10^{-13}T_g^2 + 1.092131\times10^{-17}T_g^3 - 3.661371\times10^{-2}/T_g^2)/39.95\times10^3$	NIST Chemistry WebBook
$\lambda_{g,Ar}$	W·m^{-1}·K^{-1}	$4.0\times10^{-5}T_g + 0.0054$	
$\mu_{g,Ar}$	Pa·s	$5.0\times10^{-8}T_g + 7.0\times10^{-6}$	
$\rho_{g,Ar}$	kg·m^{-3}	$1.7849\times273.15/T_g$	
ΔH_{devol}	kJ·kg^{-1}	-160.0	[45]

222 *Except for the cases listed in Tab. 3, in which the initial coal particle density $\rho_{p,0}$ is set as the tested value.

223 # 3. Experimental work

224 *3.1 Experimental scheme*

225 In the present study, two types of experiments were carried out in a specially designed lab-
226 scale bubbling fluidized bed reactor. One focused on the temperature history of a single fuel

227 particle during devolatilization in the fluidized bed. The other was designed to study the fuel
228 devolatilization characteristics including nitrogen release under different conditions.
229 The schematic diagram of this FB reactor system is shown in Fig. 3. The cylinder-shaped
230 reactor made of quartz glass is 950 mm in height with a 54 mm inner diameter and 3 mm thick
231 walls. A quartz sintered plate with a thickness of 5 mm is designed as the gas distributor and
232 fitted in the middle of the reactor. The chamber below the gas distributor where it is fully filled
233 by quartz glass fragments has the role of preheating gas. The reactor is heated electrically from
234 outside and the height of heating zone is 600 mm. Two K-type thermocouples are connected to
235 the electric heater controller and arranged outside of the reactor. A K-type thermocouple with
236 first-class precision is also immersed into the fluidizing materials to monitor the actual bed
237 temperature. During experiments, the high purity argon whose flow rate is controlled by a mass
238 flow meter enters the bed after preheating. Under different temperature conditions, the argon
239 flow rate is adjusted to keep the fluidization velocity in the same value, meanwhile, the bubbling
240 fluidization state should be ensured.

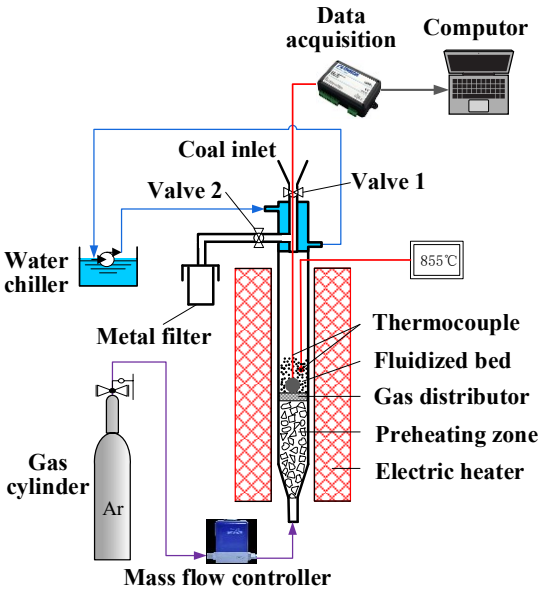

241

242 **Fig. 3 Schematic diagram of the lab-scale bubbling fluidized bed reactor**

243 Quartz sand was used as the inert bed material, and one kind of Chinese bituminous coal
244 was selected as the fuel. All coal samples were dried under 105℃ for 2h before being put into
245 the fluidized bed. The analysis of the dried coal sample is listed in Tab. 2

246 **Tab. 2 Analysis of fuel used in the laboratory experiments**

Fuel	Proximate analysis / %			Ultimate analysis / %				
	A_{ar}	V_{ar}	FC_{ar}	C_{ar}	H_{ar}	O_{ar}	N_{ar}	S_{ar}
Bituminous (dry)	10.52	39.05	49.76	64.09	4.36	18.39	1.30	0.67

247 where symbols *A*, *V*, *FC* denote mass contents of ash content, volatiles and fixed carbon in fuel,
248 respectively; *C*, *H*, *O*, *N*, *S* denote element contents of carbon, hydrogen, oxygen, nitrogen and
249 sulphur in fuel; subscript *ar* represents received base.

250 *3.2 Single fuel particle temperature history*

251 In this part of the experiments, the temperature history of the center of a single fuel particle
252 during devolatilization in a hot fluidized bed was tested. The Sauter mean diameter (D[3,2]) of

253 inert bed material was 364.1 μm. All investigated coal particles were shaped into the spherical
254 form, ranging from 10 mm to 15 mm in diameter. The relatively large size results in heat-up
255 times typically in the range 10^1 to 10^2 seconds, providing good time-resolved temperature data
256 for model evaluation. A Cr-Ni thermocouple was embedded in the particle center, following
257 which it was fastened to the particle with high-temperature sealant. This thermocouple is only
258 500 μm in diameter to minimize the effects of the attached thermocouple on the particle heating
259 process and the particles' free movement inside bed. During the test, the measured temperature
260 was recorded by a data acquisition with a sampling frequency of 3 Hz.

261 The experiments were done at 5 different conditions as listed in Tab. 3. Each case was
262 repeated three times.

263 **Tab. 3 Operating conditions in the single particle experiments**

Items	Unit	Case 1	Case 2	Case 3	Case 4	Case 5
Bed temperature	℃	750	855	955	855	855
Pyrolysis time	s	150	120	120	120	180
Coal particle diameter	mm		12		10	15
Initial coal particle mass (dry)	mg		924.2		505.8	1765.4
D[3,2] of bed material	μm			364.1		
Static bed height	mm			40		
Fluidization velocity	cm/s			26.9		
Room temperature	℃			30		

264 *3.3 Fuel pyrolysis and char preparation*

265 In this part of the experiments, char particles were prepared in a bubbling fluidized bed
266 under different temperatures. The pneumatic separation method was applied to separate the

267 pyrolytic chars from the inert bed materials. Under a specific superficial gas velocity U_g, the
268 small and light char particles with low terminal velocity $U_{p,t}$ can be entrained by gas flow,
269 while the relatively larger and heavier quartz sand particles still remain in bed. The key point
270 of this method is to select the appropriate fluidization gas velocity during the pyrolysis process
271 and pneumatic separation gas velocity, namely, the particle size of both raw fuel and quartz
272 sand should be designed well.

273 During experiments, the quartz sand with D[3,2] of 406.3 μm was used as the inert bed
274 material. Before the pyrolysis operation, the superficial gas velocity U_g was maintained at the
275 maximum pneumatic separation velocity $U_{g,se,\,max}$ for at least 15 min to remove a few small
276 inert particles in bed. Then, the U_g fell to the value that is a little higher than the minimum
277 fluidization velocity of quartz sand. A certain amount of coal particles was fed into the bed
278 through ball valve 1 and experienced the devolatilization process for 3-7 min. The $d(0.1)$, $d(0.9)$
279 and D[3,2] of raw coal particles were 219.6 μm, 571.5 μm and 332.9 μm, respectively. After
280 the devolatilization period, valve 2 was opened and valve 1 was closed. With the increase of
281 argon flow rate, different size of char particles will be carried out under different pneumatic
282 separation velocity, and all are separated by a metal filter. Finally, valve 1 was opened and
283 valve 2 was closed, and the prepared chars were collected from the filter.

284 The experiments were done at 15 different conditions as listed in Tab. 4 (five bed
285 temperature conditions, and three sizes of coal/char particles under each temperature). Each
286 case was also repeated at least three times. The proximate and ultimate analyses were done for
287 all char samples in order to study the coal devolatilization characteristics.

288 **Tab. 4 Operating conditions in the fuel particles pyrolysis experiments**

Items	Unit	Value
Pyrolysis temperature	℃	760, 810, 860, 910, 960
Pneumatic separation velocity	cm/s	40.0 (V1), 60.0 (V2), 80.0 (V3)
Pyrolysis time	min	3 (for V1), 5 (for V2), 7 (for V3)
Tested D[3,2] of char particles	μm	176.2 (d_{V1}), 284.5 (d_{V2}), 340.2 (d_{V3})
D[3,2] of bed material	μm	406.3
D[3,2] of raw coal particles	μm	332.9
Static bed height	mm	50
Room temperature	℃	20
Pyrolysis fluidization velocity	cm/s	12.0

289 # 4. Results and discussion

290 *4.1 Particle temperature history and selection principle of the heat transfer model*

291 Fig. 4 compares the calculated particle center temperature history with the experimental
292 data for five cases. The particle heat transfer model used here is the one-dimensional model.
293 For most cases, the model prediction agrees well with the experimental results, while for the
294 highest temperature results (Case 3), the 1D model is not as accurate. There are two possible
295 reasons. On the one hand, the probability of coal particle fragmentation rises with the increase
296 of bed temperature. On the other hand, the correlation equations of specific heat capacity or
297 thermal conductivity as listed in Tab. 1 may be inaccurate under high temperature, namely, the
298 thermal diffusivity is underestimated.

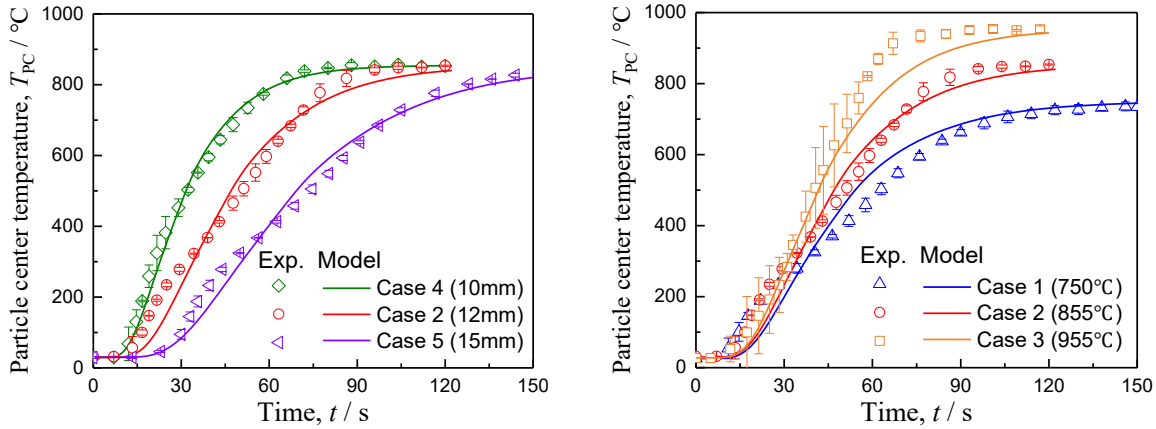

(a) Different coal particle size (T_{bed} = 855 °C) **(b) Different bed temperatures (d_p = 12 mm)**

299 **Fig. 4 Measured and 1D model predicted temperature history of the coal particles under different**

300 **conditions**

301 The stage that fuel particle local temperature increases from room temperature to 63.2%

302 of the bed temperature is defined as the rapid heating period. The average heating rate in this

303 stage under different conditions is shown in Fig. 5. It indicates that with the decrease of particle

304 size, the heating rate of the whole particle increased.

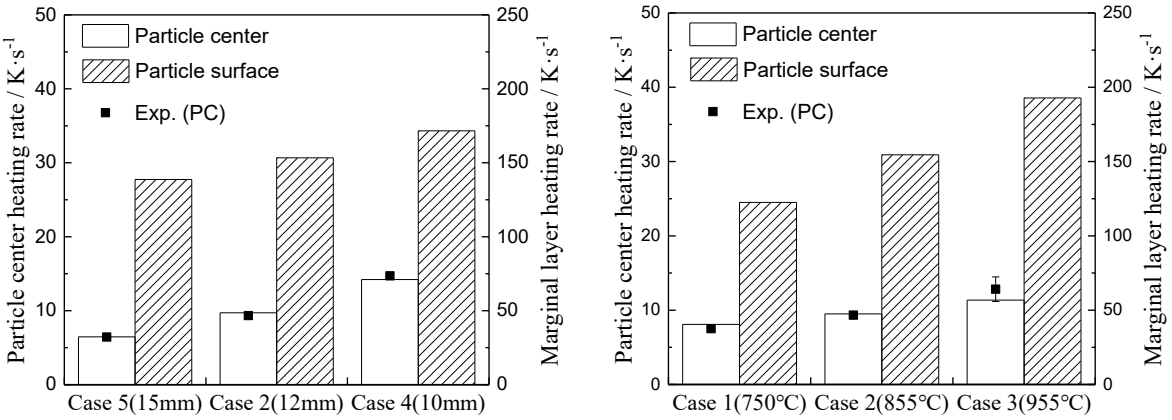

(a) Different coal particle size (T_{bed} = 855 °C) **(b) Different bed temperatures (d_p = 12 mm)**

305 **Fig. 5 Predicted heating rate in particle center and on particle surface (PS), as well as experimental**

306 **heating rate in particle center (PC) under different conditions**

Fig. 6(a) compares the particles' temperature history predicted by the two heat transfer models. It can be seen that the overall heating rate of an isothermal large particle is unrealistically high at the beginning of devolatilization process when using the 0D model. As shown in Fig. 5, the heating of the particle surface is nearly ten times faster than that of the particle center, which means the temperature distribution inside the particle is quite uneven. Therefore, for large fuel particles, the 0D isothermal particle model predicts a significantly higher devolatilization rate (see in Fig. 6(b)).

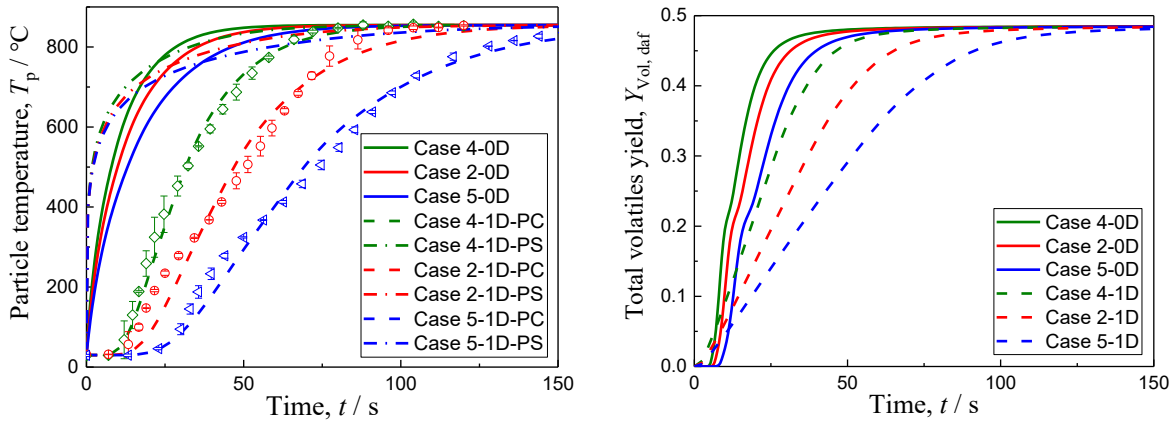

(a) Coal particle temperature history **(b) Total volatiles yield**

Fig. 6 Comparison between the results of two particle models

Fig. 7 compares the calculated results between the two heat transfer models for different sized fuel particles. The discrepancy between 0D model and 1D model becomes smaller with decreasing particle size. Considering the Biot number ($\mathrm{Bi} = h_{\mathrm{eff}} d_{\mathrm{p}} / \lambda_{\mathrm{p}}$), the small particle usually has a small Bi value, namely, the heat transfer resistance inside a particle is much lower than that in the surface, and this particle can be described as isothermal.

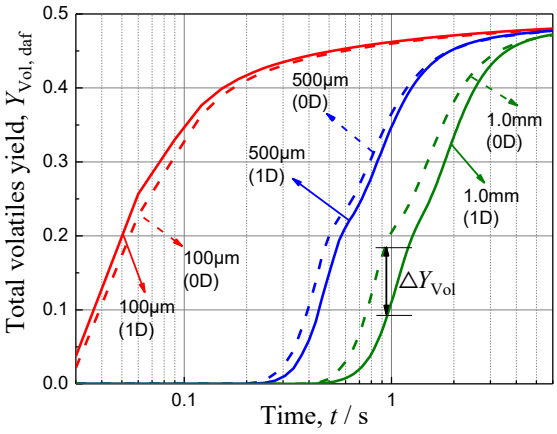

320

321 **Fig. 7 The discrepancy of volatiles yield history between the results of two particle models (T_{bed} =**

322 **850℃)**

323 To quantify the difference between the models, the time integration deviation of total

324 volatiles yield between the two models is defined:

325 $$\delta_{0D\text{-}1D} = \frac{\int_{t=0}^{t_{devol}} \left| Y_{Vol,daf,1D}(t) - Y_{Vol,daf,0D}(t) \right| dt}{\int_{t=0}^{t_{devol}} Y_{Vol,daf,1D}(t)\, dt} \approx \frac{\sum_{k=1}^{N_k} \left(\Delta t_{(k)} \left| Y_{Vol,daf,1D(k)} - Y_{Vol,daf,0D(k)} \right| \right)}{\sum_{k=1}^{N_k} \left(\Delta t_{(k)} Y_{Vol,daf,1D(k)} \right)} \quad (14)$$

326 where t_{devol} denotes the devolatilization time.

327 Under different bed temperatures, the variation of $\delta_{0D\text{-}1D}$ with particle size is shown in Fig.

328 8:

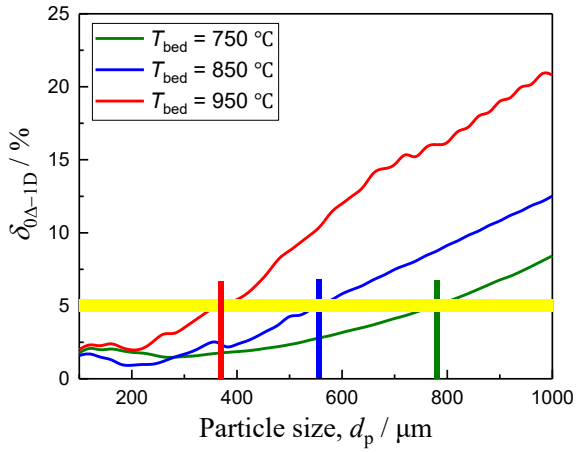

329

330 **Fig. 8 The time integration deviation of total volatiles yield between two particle models, with 5%**

331 **deviation threshold indicated**

332 It shows that the $\delta_{0D\text{-}1D}$ is lower than 5% when the particle size does not exceed a specific

333 value (transition size). However, as the size increases further, the deviation between these two

334 heat transfer models grows significantly which cannot be ignored. In addition, this transition

335 size is related to the environmental temperature, T_g. Under higher temperatures, the deviation

336 $\delta_{0D\text{-}1D}$ is larger and the transition size should be smaller. It can also be explained by the Biot

337 number. The integrated external heat transfer coefficient over particle surface h_{eff} is written as

338 follows:

339 $$h_{eff} = h_{gc} + h_{pc} + \frac{\kappa_p \sigma \left(T_g^4 - T_p^4\right)}{T_g - T_p} \quad (15)$$

340 The higher the T_g, the larger the h_{eff} is. While for the same size fuel particles, the internal heat

341 transfer resistance, d_p/λ_p, is a weaker function of temperature. Therefore, the Biot number is

342 greater under higher environmental temperature, namely, the particle inside temperature is more

343 uneven. Fig. 5(b) also shows that with the increase of bed temperature, the particle surface

344 heating rate increases more as compared to the particle center heating rate.

345 Within the bed temperature range 750℃ ~ 950℃, the transition size $d_{p,0D\text{-}1D}$ can be
346 approximated by a linear relationship based on Fig. 8:

347 $$d_{tr,0D-1D}\left(\mu m\right) = -2T_g\left(K\right) + 2800 \quad (16)$$

348 For some types of FB reactors such as the CFB boiler, the feeding fuel size usually covers
349 a wide range (10^0 μm ~ 10^3 μm). On the other hand, the calculation of 1D particle
350 devolatilization model takes much more time than the 0D model does. Considering both the
351 calculation precision and computational efficiency, in the present work, the 1D particle model
352 is applied when the particle size is larger than $d_{tr,0D\text{-}1D}$, while the isothermal particle model is
353 used for the smaller fuel particles. The hybrid 0D/1D particle model is used in the section to
354 follow, which focuses on experimental measurement and model predictions of fuel
355 devolatilization characteristics.

356 *4.2 The effect of particle size and temperature on fuel devolatilization characteristics*

357 All char samples which were prepared in a bubbling fluidized bed following the method
358 introduced in section 3.3 were tested to obtain their elemental analysis data. Fig. 9 shows that
359 the hydrogen content in char decreases with temperature. This trend is consistent with the
360 results of some other studies: whether coal or biomass, more volatiles are released at higher
361 temperature [22, 35].

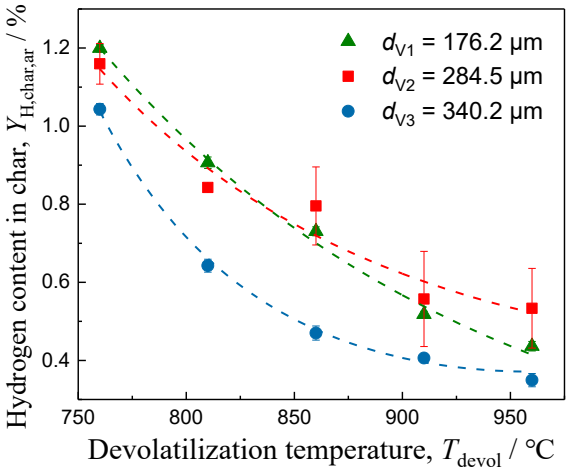

362

363 **Fig. 9 Experimental hydrogen content in char at different temperatures (w_t -%)**

364 The experimental results published by Sadhukhan et al. [3] are also used to validate the

365 devolatilization model developed in this paper. Five particle sizes (0.92mm, 2.18mm, 3.0mm,

366 4.36mm, 6.0mm) and two bed temperatures (700 ℃, 850 ℃) are chosen in their studies. Fig.

367 10 compares the final volatiles yield and devolatilization time obtained in Sadhukhan et al.'s

368 experiments with the model predictions in this paper.

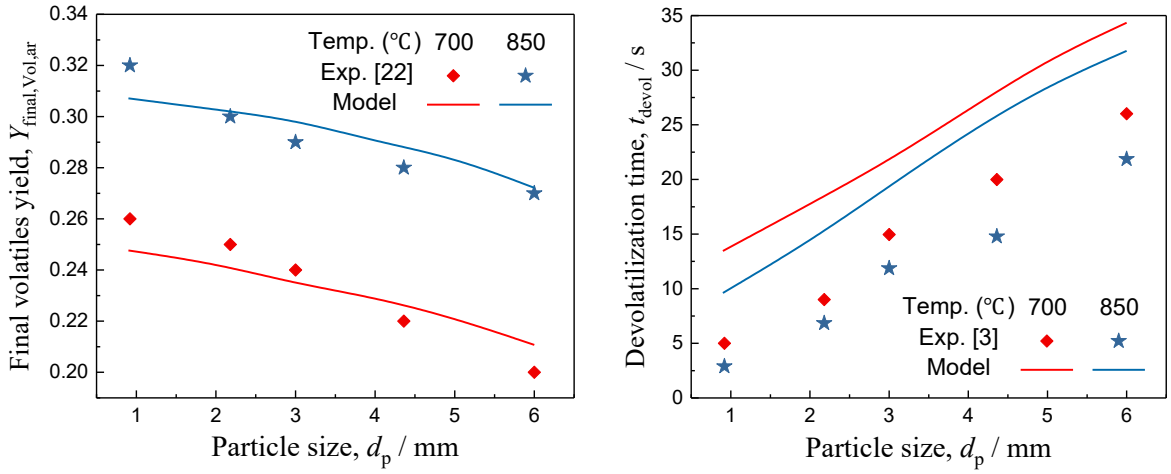

(a) Final volatiles yield (N_2 atmosphere) **(b) Devolatilization time (Air atmosphere)**

369 **Fig. 10 Comparison of predicted and experimentally obtained devolatilization behavior in a**

370 **fluidized bed**

371 The model prediction of the final volatiles yield agrees well with the experimental results.
372 However, the predicted devolatilization time is generally longer than the experimental one. The
373 difference appears to be an almost constant offset, independent of particle size. A possible
374 explanation for it is the difference in the definition of devolatilization time. In the study of
375 Sadhukhan et al., the disappearance moment of volatile flame is regarded as the end of
376 devolatilization, while after that, the volatiles may continue to be released slowly. Another
377 possible reason is that the thermal conductivity, specific heat capacity and particle density
378 depend on the fuel types, namely, the thermal diffusivity varies from coal to coal which has
379 significant effect on the particle heat-up process.

380 Both experimental and model results reveal that the mass loss is a little higher for smaller
381 fuel particles. As mentioned in section 4.1, the fuel heating rate is increased with the decrease
382 of particle size. Yan et al found that the fast pyrolysis of coal slightly increases the coal
383 conversion compared to the slow pyrolysis process [17], which may be the reason for the above
384 phenomenon.

385 Fig. 11 compares the experimentally obtained normalized N/C ratio in char ($\theta_{N/C}$, which
386 is expressed in Equ.(2)) with the model predictions. Though the trend is the same, the original
387 CPD-NLG model significantly underestimated the nitrogen release fraction. To correct this
388 deviation, some modifications to the nitrogen release chemical kinetic parameters in CPD-NLG
389 model should be made.

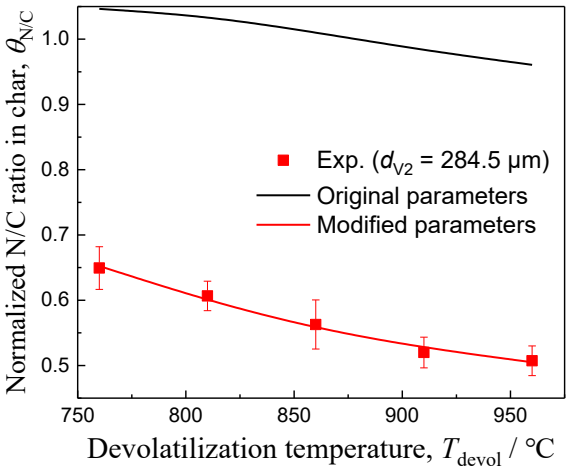

390

391 **Fig. 11 Comparison of two NLG model predicted $\theta_{N/C}$ with the experimental results**

392 In the CPD-NLG model, the nitrogen release from coal includes three main pathways: a)
393 Nitrogen-containing tar clusters leave away from char during tar release. b) Breakage of ring
394 nitrogen in char that occurs quickly at temperatures lower than 1600 K (fast light gas nitrogen
395 release). c) Ring nitrogen is slowly broken out of the char clusters at pretty high temperatures
396 (slow light gas nitrogen release). Pathway A is controlled by the tar release mechanism that is
397 described by the CPD model, and the required reaction temperature for pathway C is usually
398 higher than the temperature in most FB reactors. Therefore, only the reaction rate for pathway
399 B is adjusted in this paper.

400 The overall global rate expression for pathway B is written as [13, 15]:

401 $$\frac{d\left(N_{site}\right)}{dt} = k_N \frac{M_{site}}{\left(M_{cl}\right)^2} \frac{d\left(M_{cl}\right)}{dt} N_{site} \tag{17}$$

402 where N_{site} denotes the ring nitrogen concentration, M_{site} denotes the aromatic mass per cluster,
403 M_{cl} denotes the total mass per cluster. The specific meaning and calculated method of these
404 parameters are found elsewhere [13, 15].

405 The reaction rate k_N in the original NLG model is expressed as the Arrhenius form with
406 constant activation energy. While, in this paper, this reaction is assumed to have a distributed
407 activation energy:

408 $$k_N = A_N \exp\left(-\left[\left(E_N \pm V_N\right)/RT\right]\right) \quad (18)$$

409 where A_N, E_N and V_N are the pre-exponential frequency factor, the activation energy and the
410 distributed variation in activation energy. The normalized probability function and the
411 calculation method for the distributed activation energy can refer to Ref. [12], which is also
412 applied for the other reactions in the CPD model.

413 The value of these three kinetic parameters, A_N (=20.0), E_N (=18.8 kJ/mol) and V_N (=2.1
414 kJ/mol), were obtained by fitting the present experimental data. Fig. 11 and Fig. 12 show the
415 results of the modified NLG model.

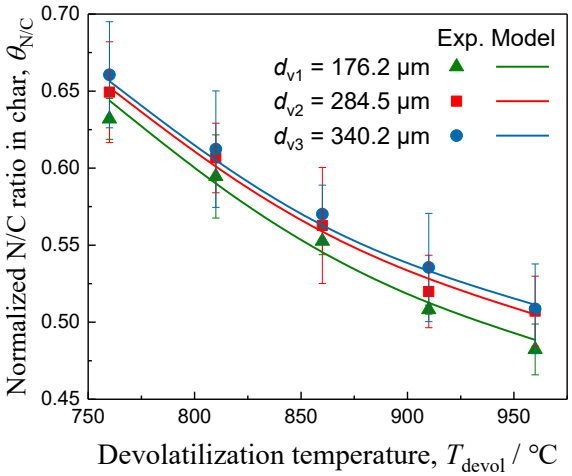

416

417 **Fig. 12 Normalized N/C ratio of char at different devolatilization temperature and particle size**

418 Fig. 12 illustrates the $\theta_{N/C}$ versus devolatilization temperature for different size coal
419 particles. The results imply that at a high degree of devolatilization, i.e. high final temperature
420 or faster heating rate (smaller particles), the final nitrogen content in char will be decreased,

421 namely, more nitrogen will be released as volatiles. This phenomenon is also shown in many
422 studies [13, 46-48]. However, the $\theta_{N/C}$ is less than 1.0 in all cases. This observation is
423 inconsistent with some reported results that the nitrogen enrichment in char generally occurs in
424 the range of 600-1200 K [2, 13, 27]. However, also some studies show that the ratio of volatile-
425 N to fuel-N can be higher than the volatile matter content in some conditions [47, 48], which is
426 in line with the results of the present work. Kambara et al. [48] investigated the formation of
427 NO_x precursors during rapid pyrolysis for 20 coals covering a wide temperature range (853-
428 1488 K). He found that the yields of volatile-N are strongly dependent on coal types, and it is
429 uncertain whether the char is enriched in nitrogen for different fuels.

430 One issue should be pointed out here. The deviation between the calculation results using
431 original or modified chemical kinetic parameters (as shown in Fig. 11) can be attributed to two
432 main reasons. On the one hand, as mentioned above, the yields of volatile-N are strongly
433 dependent on coal types, namely, the chemical kinetic parameters for different fuels are
434 discrepant. On the other hand, the type of reactor is different. In this paper, the reactor is a
435 bubbling fluidized bed, in other studies it may be a drop tube furnace or a fixed bed reactor.
436 Actually, the physical processes involved in a fluidized bed are relatively complex, including
437 not only the heat transfer, but also the gas-solid two-phase flow and mass transfer, thus some
438 factors that are related to the reactor itself may be ignored here. However, it cannot say that the
439 original parameters reported by Perry are inaccurate, by contrast, they are more universal since
440 these original parameters were regressed using a collection of more different coals [13, 15].
441 The parameters obtained in this paper are just more suitable for this kind of coal and the

fluidized bed conditions. From another perspective, the coal devolatilization characteristics, including the ratio of volatile-N to total fuel-N, have significant effect on the final NO_x emission of a FB reactor. Hence, the chemical kinetic parameters about nitrogen release should be determined carefully in modeling.

Fig. 13 shows the predicted yields of tar and light gas of different size coal particles at three devolatilization temperatures. The simulation conditions for this figure is the same as listed in Tab. 3.

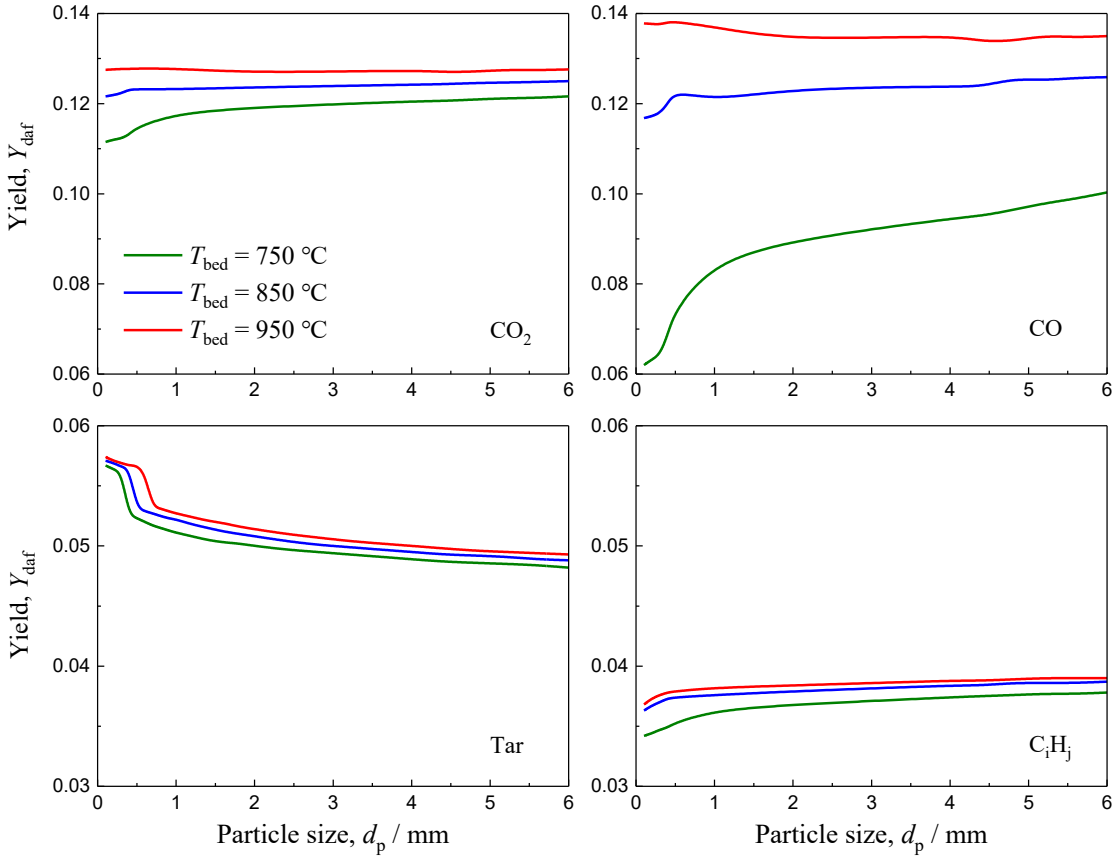

Fig. 13 The simulated yields of selected volatile species as a function of coal particle size and devolatilization temperature

The simulation shows that if the bed temperature increases, the yields of all volatile species will increase in varying degrees. The experimental results reported in some literature show that

454 the yield of CO significantly increases with the increase of devolatilization temperature [17, 19,
455 21, 31, 37]. However, the rising trend for other light gases is not so obvious as CO [37], even
456 the yields are unchanged or slightly decrease at higher temperatures [17, 19, 21]. These trends
457 are also shown in Fig. 13. In addition, as the coal particle size increases, the yield of tar
458 decreases and the yields of other light gaseous species increase, which is in general agreement
459 with the findings reported in literature [23, 33, 47]. Meanwhile, this variation tendency is only
460 obvious in the small size range. Shen et al. [33] also found that in a FB reactor, the yield of bio-
461 oil only decreases when the biomass particle size increases from 0.3 to 1.5 mm, further increases
462 in particle size has a negligible effect on the bio-oil yield. It is mainly attributed to the variation
463 of heating rate among different size fuel particles.

464 *4.3 Sensitivity analysis*

465 The temperature evolution of fuel particle during devolatilization is affected by various
466 fuel properties, involving specific heat capacity (c_p), thermal conductivity (λ_p), particle density
467 (ρ_p) and enthalpy of devolatilization (ΔH_{devol}), etc. The extent of the impact of each parameter
468 is discrepant. A sensitivity analysis is carried out, taking as a reference the average heating rate
469 in particle center during rapid heating period and the normalized N/C ratio in char. Fig. 14
470 shows the results of sensitivity analysis, obtained by increasing and decreasing each parameter
471 by 25%.

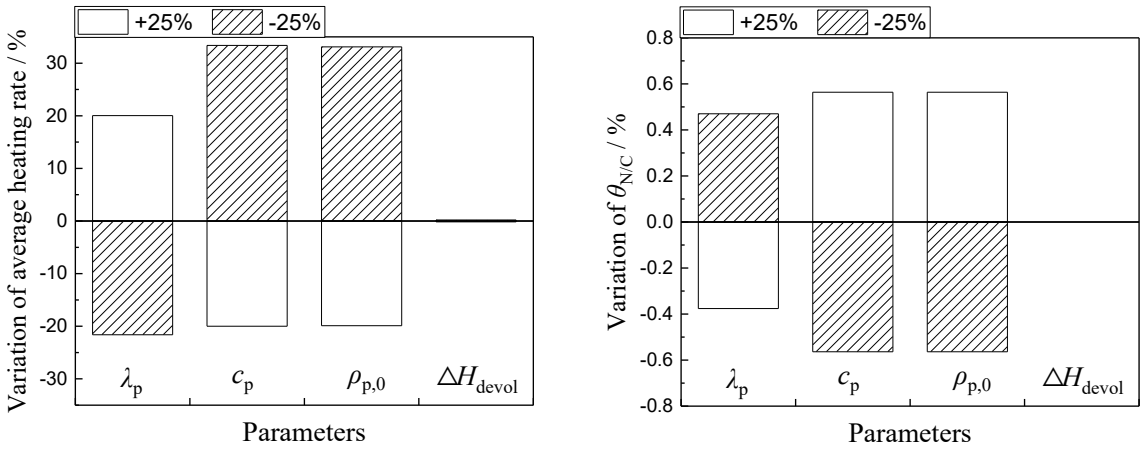

(a) Average heating rate **(b) Normalized N/C ratio in char**

Fig. 14 Parameter sensitivity analysis of the model (conditions of case 2 as listed in Tab. 3)

It shows that the coal particle heating process as well as the devolatilization behavior is insensitive to the ΔH_{devol}. It is because that compared to the overall heat transfer from outside environment (gas/solid convection and radiation), the heat loss due to the enthalpy of devolatilization is much smaller. The item $dm_{Vol}/dt \cdot \Delta H_{devol}$ is even ignored in some literature [8].

However, the particle's specific heat capacity, thermal conductivity and density, namely, the thermal diffusivity ($\alpha_p = \lambda_p/(\rho_p c_p)$), show significant influence on the fuel particle heat-up process. Due to the difference in pore structure, element content, mineral composition and some other properties, the thermal diffusivity varies considerably among fuels. If λ_p increases, c_p decreases or ρ_p decreases, the α_p will be higher and the particle temperature will rise quickly, thus the devolatilization characteristics may be also affected, for example, more fuel nitrogen tends to be released as volatiles. This may be one of the reasons that different types of fuel differ in devolatilization characteristics.

5. Conclusion

In this study, two different mathematical models, isothermal (0D) particle model and one-dimensional (1D) particle model, have been developed for predicting fuel particle heat-up and devolatilization behavior in a fluidized bed. The particle heat transfer is solved simultaneously using an iterative approach with the existing CPD-NLG model. Experiments in a special designed lab-scale FB reactor were conducted to help validate both the temperature solver and modifications to the fast nitrogen release chemical kinetic parameters. Though the 0D particle model is not suitable for large fuel particles and may overestimate the devolatilization rate, the deviation between the results of these two particle models can be acceptably small if the particle size is smaller than a specific value (transition size), and this transition size decreases with the increase of environmental temperature. For a FB reactor with a wide size range of feeding fuel, a selection principle of the 1D or 0D particle model is proposed based on the fuel particle size and bed temperature, in order to obtain a good balance between the calculation precision and computational efficiency.

Both experimental and model results show that at a high degree of devolatilization, i.e. high final temperature or faster heating rate (smaller particles), the final volatiles yield increases and the nitrogen remaining in char decreases. In addition, under all conditions given in the present experiment, the final nitrogen content of the char is lower than that of the parent coal. Finally, based on the developed devolatilization model, the effects of fuel particle size and temperature on the yields of some volatile species are discussed. The particle model developed

506 in this work makes it possible to carry out future FB reactor calculations with the
507 devolatilization process more consistent with laboratory data.

508 ## Nomenclature

Abbreviation

FB	fluidized bed
CPD	chemical percolation devolatilization (model)
NLG	nitrogen and light gas (model)

Symbols

A	area (m^2), pre-exponential frequency factor (-)
Bi	Biot number (-)
c	specific heat capacity ($J \cdot kg^{-1} \cdot K^{-1}$)
c_0	initial fraction of char bridges
D	diffusion coefficient ($m^2 \cdot s^{-1}$)
d	particle size (μm, mm, m)
E	activation energy ($kcal \cdot mol^{-1}$)
h	heat transfer coefficient ($W \cdot m^{-2} \cdot K^{-1}$)
k	reaction rate (-)
M_{site}	aromatic mass per cluster (-)
M_{cl}	total mass per cluster (-)

M_{del}	side chain molecular weight (-)
m	mass (kg)
N	number (-)
N_s	surface thermal contact resistance constant (-)
Nu	Nusselt number (-)
N_{site}	ring nitrogen concentration (mol)
Pr	Prandtl number (-)
p_0	initial fraction of bridges in the coal lattice
Q	heat flow (W)
R	thermal resistance ($m^2 \cdot K \cdot W^{-1}$), gas constant ($kcal \cdot mol \cdot K^{-1}$)
Re	Reynolds number (-)
r	radius (m)
T	temperature (K)
t	time (s)
U	velocity ($m \cdot s^{-1}$)
V	distributed variation in activation energy ($kcal \cdot mol^{-1}$)
Y	mass fraction of volatiles, or elements, or other matters (-)
ΔH	latent heat ($J \cdot kg^{-1}$)
ρ	density ($kg \cdot m^{-3}$)
ε	voidage (-)
γ_{daf}	content of char plus volatiles (-)

$\theta_{N/C}$	normalized N/C ratio in the char (-)
θ_t	mean emulsion residence time (s)
φ_N	mass fraction of original nitrogen remaining in the char
κ	effective surface emissivity (-)
σ	Stefan-Boltzmann constant ($W \cdot m^{-2} \cdot K^{-4}$)
$\sigma + 1$	lattice coordination number (-)
μ	dynamic viscosity ($Pa \cdot s$)
λ	heat conduction coefficient ($W \cdot m^{-1} \cdot K^{-1}$)
χ_V	volume fraction of particle layer (-)
$\delta_{0D\text{-}1D}$	time integration deviation between two heat transfer models (-)

Subscripts

ar	in received basis
daf	in dry ash-free basis
devol	devolatilization
e	environment
em	emulsion phase
g	gas phase
gc	gas convection
j	particle group
k	particle age group

l	particle layer number
ML	particle marginal layer
m	volatile species number
mf	minimum fluidization state
N	nitrogen
p	single fuel particle
PC	particle center
sc	solid particle convection
r	radiation
s	solid bed materials
tr	transition
Vol	volatiles

Acknowledgment

This work was supported by the National Natural Science Foundation of China (U1810126). Mr. Xiwei Ke also acknowledges the Johan Gadolin Process Chemistry Centre (PCC) in Åbo Akademi University for the Johan Gadolin Scholarship (JGS) awarded.

References

[1] Bu C, Leckner B, Chen X, Pallarès D, Liu D, Gómez-Barea A. Devolatilization of a single fuel particle in a fluidized bed under oxy-combustion conditions. Part A: Experimental results. Combustion and Flame. 2015;162:797-808.

[2] Phiri Z, Everson RC, Neomagus HWJP, Engelbrecht AD, Wood BJ, Nyangwa B. Release of Nitrogenous Volatile Species from South African Bituminous Coals during Pyrolysis. Energy Fuels. 2018;32:4606-4616.
[3] Sadhukhan AK, Gupta P, Saha RK. Modeling and experimental studies on single particle coal devolatilization and residual char combustion in fluidized bed. Fuel. 2011;90:2132-2141.
[4] Baum MM, Street PJ. Predicting the Combustion Behaviour of Coal Particles. Combustion Science and Technology. 1971;3:231-243.
[5] Badzioch S, Hawksley PGW. Kinetics of Thermal Decomposition of Pulverized Coal Particles. Ind Eng Chem Process Design and Development. 1970;9:521-530.
[6] Kobayashi H, Howard JB, Sarofim AF. Coal Devolatilization at High Temperatures. In 16th Symposium (Int'I) on Combustion. 1976.
[7] Anthony DB, Howard JB. Coal DevoIatiIization and Hydrogasification. AICHE J. 1976;22:625-656.
[8] Bu C, Leckner B, Chen X, Gómez-Barea A, Liu D, Pallarès D. Devolatilization of a single fuel particle in a fluidized bed under oxy-combustion conditions. Part B: Modeling and comparison with measurements. Combustion and Flame. 2015;162:809-818.
[9] Chen D, Jiang X. Fluidized Bed Drying and Devolatilization of Lignite Washery Tailing Particles: Experiments and Modeling. Energy Fuels. 2018;32:11887-11898.
[10] Fletcher TH, Kerstein AR, Pugmire RJ, Solum MS, Grant DM. Chemical percolation model for devolatilization. 3. direct use of 13C NMR data to predict effects of coal type. Energy Fuels. 1992;6:414-431.
[11] Fletcher TH, Kerstein AR, Pugmire RJ, Grant DM. Chemical percolation model for devolatilization. 2. temperature and heating rate effects on product yields. Energy Fuels. 1990;4:54-60.
[12] Grant DM, Pugmire RJ, Fletcher TH, Kerstein AR. Chemical Model of Coal Devolatilization Using Percolation Lattice Statistics. Energy Fuels. 1989;3:175-186.
[13] Perry ST, Fletcher TH. Modeling Nitrogen Evolution during Coal Pyrolysis Based on a Global Free-Radical Mechanism. Energy Fuels. 2000;14:1094-1102.
[14] Zhang H. Nitrogen evolution and soot formation during secondary coal pyrolysis. Brigham Young University: Brigham Young University; 2001.
[15] Perry ST. A global free-radical mechanism for nitrogen release during coal devolatilization based on chemical structure. Brigham Young University: Brigham Young University; 1999.
[16] Salmasi A, Shams M, Chernoray V. Simulation of sub-bituminous coal hydrodynamics and thermochemical conversion during devolatilization process in a fluidized bed. Applied Thermal Engineering. 2018;135:325-333.
[17] Yan B-H, Cao C-X, Cheng Y, Jin Y, Cheng Y. Experimental investigation on coal devolatilization at high temperatures with different heating rates. Fuel. 2014;117:1215-1222.
[18] Lewis AD, Fletcher TH. Prediction of Sawdust Pyrolysis Yields from a Flat-Flame Burner Using the CPD Model. Energy Fuels. 2013;27:942-953.
[19] Fuentes-Cano D, Salinero J, Haro P, Nilsson S, Gómez-Barea A. The influence of volatiles to carrier gas ratio on gas and tar yields during fluidized bed pyrolysis tests. Fuel. 2018;226:81-86.

[20] Tian B, Qiao Y, Fan J, Bai L, Tian Y. Coupling Pyrolysis and Gasification Processes for Methane-Rich Syngas Production: Fundamental Studies on Pyrolysis Behavior and Kinetics of a Calcium-Rich High-Volatile Bituminous Coal. Energy Fuels. 2017;31:10665-10673.
[21] Neves D, Matos A, Tarelho L, Thunman H, Larsson A, Seemann M. Volatile gases from biomass pyrolysis under conditions relevant for fluidized bed gasifiers. Journal of Analytical and Applied Pyrolysis. 2017;127:57-67.
[22] Jayaraman K, Kok MV, Gokalp I. Pyrolysis, combustion and gasification studies of different sized coal particles using TGA-MS. Applied Thermal Engineering. 2017;125:1446-1455.
[23] Tian B, Qiao Yy, Tian Yy, Liu Q. Investigation on the effect of particle size and heating rate on pyrolysis characteristics of a bituminous coal by TG–FTIR. Journal of Analytical and Applied Pyrolysis. 2016;121:376-386.
[24] Zhou H, Huang Y, Mo G, Liao Z, Cen K. Experimental investigations of the conversion of fuel-N, volatile-N and char-N to NOx and N2O during single coal particle fluidized bed combustion. Journal of the Energy Institute. 2017;90:62-72.
[25] Li P-W, Chyang C-S, Ni H-W. An experimental study of the effect of nitrogen origin on the formation and reduction of NOx in fluidized-bed combustion. Energy. 2018;154:319-327.
[26] He J, Song W, Gao S, Dong L, Barz M, Li J, et al. Experimental study of the reduction mechanisms of NO emission in decoupling combustion of coal. Fuel Processing Technology. 2006;87:803-810.
[27] Johnsson JE. Formation and reduction of nitrogen oxides in fluidized-bed combustion. Fuel. 1994;73:1398-1415.
[28] Konttinen J, Kallio S, Hupa M, Winter F. NO formation tendency characterization for solid fuels in fluidized beds. Fuel. 2013;108:238-246.
[29] Ström H, Thunman H. A computationally efficient particle submodel for CFD-simulations of fixed-bed conversion. Applied Energy. 2013;112:808-817.
[30] Chen J, Fang D, Duan F. Pore characteristics and fractal properties of biochar obtained from the pyrolysis of coarse wood in a fluidized-bed reactor. Applied Energy. 2018;218:54-65.
[31] Valdés CF, Chejne F. Effect of reaction atmosphere on the products of slow pyrolysis of coals. Journal of Analytical and Applied Pyrolysis. 2017;126:105-117.
[32] Ren Q, Zhao C, Wu X, Liang C, Chen X, Shen J, et al. Formation of NOx precursors during wheat straw pyrolysis and gasification with O2 and CO2. Fuel. 2010;89:1064-1069.
[33] Shen J, Wang X-S, Garcia-Perez M, Mourant D, Rhodes MJ, Li C-Z. Effects of particle size on the fast pyrolysis of oil mallee woody biomass. Fuel. 2009;88:1810-1817.
[34] Ruben Sudhakar D, Kolar AK. Experimental investigation of the effect of initial fuel particle shape, size and bed temperature on devolatilization of single wood particle in a hot fluidized bed. Journal of Analytical and Applied Pyrolysis. 2011;92:239-249.
[35] Salmasi A, Shams M, Chernoray V. An experimental approach to thermochemical conversion of a fuel particle in a fluidized bed. Applied Energy. 2018;228:524-534.
[36] Zhang G, Zhu C, Ge Y, Liu X, Xu G. Fluidized bed combustion in steam-rich atmospheres for high-nitrogen fuel: Nitrogen distribution in char and volatile and their contributions to NOx. Fuel. 2016;186:204-214.

[37] Kawabata Y, Nakagome H, Wajima T, Hosokai S, Sato H, Matsuoka K. Tar Emission during Pyrolysis of Low Rank Coal in a Circulating Fluidized Bed Reactor. Energy Fuels. 2018;32:1387-1394.
[38] Genetti D, Fletcher TH, Pugmire RJ. Development and Application of a Correlation of 13C NMR Chemical Structural Analyses of Coal Based on Elemental Composition and Volatile Matter Content. Energy Fuels. 1999;13:60-68.
[39] Baskakov AP, Berg BV, Vitt OK, Filippovsky NF, Kirakosyan VA, Goldobin JM, et al. Heat transfer to objects immersed in fluidized beds. Powder Technology. 1973;8: 273-282.
[40] Baskakov AP, Leckner B. Radiative heat transfer in circulating fluidized bed furnace. Powder Technology. 1997;90: 213-218.
[41] Geldart D, Cullinan J, Georghiades S. The effect of fines on entrainment from gas fluidized beds. Transactions of the Institution of Chemical Engineers. 1979;57:269-275.
[42] Chao J, Lu J, Yang H, Zhang M, Liu Q. Experimental study on the heat transfer coefficient between a freely moving sphere and a fluidized bed of small particles. International Journal of Heat and Mass Transfer. 2015;80:115-125.
[43] Chen Q, Zhang G, Qin R, Tang M. Measurements of Thermal Conductivity and Diffusivity of Loose Coal Using a Hot-Wire Method. Journal of China University of Mining &Technology. 2009;38:336-340.
[44] Li J.J., Yang X.H., Yang H.R., Lyu J.F., Experimental study and modeling of NOx generation from char nitrogen in the bubbling bed. Journal of China Coal Society. 2016;41:1546-1553.
[45] J. Tomeczek and H. Palugniok, Specific heat capacity and enthalpy of coal pyrolysis at elevated temperatures. Fuel. 1996;75:1089-1093.
[46] Becidan M, Skreiberg Ø, Hustad JE. NOx and N_2O precursors (NH_3 and HCN) in pyrolysis of biomass residues. Energy Fuels. 2007;21:1173-1180.
[47] Leppalahti J. Formation of NH3 and HCN in slow-heating-rate inert pyrolysis of peat, coal and bark. Fuel. 1995;74:1363-1368.
[48] Kambara S, Takarada T, Yamamoto Y, Kato K. Relation between functional forms of coal nitrogen and formation of NOx precursors during rapid pyrolysis. Energy Fuels. 1993;7:1013-1020.
[49] Kang B-S, Lee KH, Park HJ, Park Y-K, Kim J-S. Fast pyrolysis of radiata pine in a bench scale plant with a fluidized bed: Influence of a char separation system and reaction conditions on the production of bio-oil. Journal of Analytical and Applied Pyrolysis. 2006;76:32-37.